

University of Groningen

Probing size variations of molecular aggregates inside chlorosomes using single-object spectroscopy

Kunsel, T.; Günther, L. M.; Köhler, J.; Jansen, T. L. C.; Knoester, J.

Published in:
Journal of Chemical Physics

DOI:
[10.1063/5.0061529](https://doi.org/10.1063/5.0061529)

IMPORTANT NOTE: You are advised to consult the publisher's version (publisher's PDF) if you wish to cite from it. Please check the document version below.

Document Version
Publisher's PDF, also known as Version of record

Publication date:
2021

[Link to publication in University of Groningen/UMCG research database](#)

Citation for published version (APA):

Kunsel, T., Günther, L. M., Köhler, J., Jansen, T. L. C., & Knoester, J. (2021). Probing size variations of molecular aggregates inside chlorosomes using single-object spectroscopy. *Journal of Chemical Physics*, 155(12), [124310]. <https://doi.org/10.1063/5.0061529>

Copyright

Other than for strictly personal use, it is not permitted to download or to forward/distribute the text or part of it without the consent of the author(s) and/or copyright holder(s), unless the work is under an open content license (like Creative Commons).

The publication may also be distributed here under the terms of Article 25fa of the Dutch Copyright Act, indicated by the "Taverne" license. More information can be found on the University of Groningen website: <https://www.rug.nl/library/open-access/self-archiving-pure/taverne-amendment>.

Take-down policy

If you believe that this document breaches copyright please contact us providing details, and we will remove access to the work immediately and investigate your claim.

Downloaded from the University of Groningen/UMCG research database (Pure): <http://www.rug.nl/research/portal>. For technical reasons the number of authors shown on this cover page is limited to 10 maximum.

Probing size variations of molecular aggregates inside chlorosomes using single-object spectroscopy


Cite as: J. Chem. Phys. **155**, 124310 (2021); <https://doi.org/10.1063/5.0061529>

Submitted: 27 June 2021 • Accepted: 26 August 2021 • Published Online: 29 September 2021

 T. Kunsel,  L. M. Günther,  J. Köhler, et al.

COLLECTIONS

 This paper was selected as Featured

 This paper was selected as Scilight



View Online



Export Citation



CrossMark

ARTICLES YOU MAY BE INTERESTED IN

[Scaling relations of exciton diffusion in linear aggregates with static and dynamic disorder](#)
The Journal of Chemical Physics **155**, 134305 (2021); <https://doi.org/10.1063/5.0065206>

[Computational spectroscopy of complex systems](#)
The Journal of Chemical Physics **155**, 170901 (2021); <https://doi.org/10.1063/5.0064092>

[Light sizes up the internal structure of chlorosomes](#)
Scilight **2021**, 401104 (2021); <https://doi.org/10.1063/10.0006618>

 **The Journal of Chemical Physics** **Special Topics** Open for Submissions [Learn More](#)

Probing size variations of molecular aggregates inside chlorosomes using single-object spectroscopy



Cite as: *J. Chem. Phys.* **155**, 124310 (2021); doi: [10.1063/5.0061529](https://doi.org/10.1063/5.0061529)

Submitted: 27 June 2021 • Accepted: 26 August 2021 •

Published Online: 29 September 2021



View Online



Export Citation



CrossMark

T. Kunsel,¹ L. M. Günther,² J. Köhler,^{2,3,4} T. L. C. Jansen,¹ and J. Knoester^{1,a)}

AFFILIATIONS

¹University of Groningen, Zernike Institute for Advanced Materials, Nijenborgh 4, 9747 AG Groningen, The Netherlands

²Spectroscopy of Soft Matter, University of Bayreuth, Universitätsstraße 30, D-95440 Bayreuth, Germany

³Bavarian Polymer Institute, University of Bayreuth, Universitätsstraße 30, D-95440 Bayreuth, Germany

⁴Bayreuth Institute of Macromolecular Research (BIMF), University of Bayreuth, Universitätsstraße 30, D-95440 Bayreuth, Germany

^{a)}Author to whom correspondence should be addressed: j.knoester@rug.nl

ABSTRACT

We theoretically investigate the possibility to use single-object spectroscopy to probe size variations of the bacteriochlorophyll aggregates inside chlorosomes. Chlorosomes are the light-harvesting organelles of green sulfur and non-sulfur bacteria. They are known to be the most efficient light-harvesting systems in nature. Key to this efficiency is the organization of bacteriochlorophyll molecules in large self-assembled aggregates that define the secondary structure inside the chlorosomes. Many studies have been reported to elucidate the morphology of these aggregates and the molecular packing inside them. It is widely believed that tubular aggregates play an important role. Because the size (radius and length) of these aggregates affects the optical and excitation energy transport properties, it is of interest to be able to probe these quantities inside chlorosomes. We show that a combination of single-chlorosome linear polarization resolved spectroscopy and single-chlorosome circular dichroism spectroscopy may be used to access the typical size of the tubular aggregates within a chlorosome and, thus, probe possible variations between individual chlorosomes that may result, for instance, from different stages in growth or different growth conditions.

Published under an exclusive license by AIP Publishing. <https://doi.org/10.1063/5.0061529>

I. INTRODUCTION

Photosynthesis is one of the most important processes to sustain life on earth. The biomolecular systems and mechanisms that underlie photosynthesis have been the subject of many studies, which not only serve fundamental interest but also are sources of inspiration for technological applications.^{1–6} Investigations of the initial absorption of sunlight in natural light-harvesting systems and the subsequent excitation energy transport to photosynthetic reaction centers guide the selection and design of synthetic supramolecular materials that mimic these functions.^{7–9} Among the natural light-harvesting systems, the chlorosome, which is the antenna system of green sulfur and non-sulfur bacteria, has attracted particular attention. It owes this interest to the fact that it is the most efficient light-harvesting system known in nature^{10,11} and that in contrast to other light-harvesting systems,^{10,12} it contains molecular

aggregates that are self-assemblies of only bacteriochlorophyll (BChl) molecules, i.e., they lack complicated protein scaffolds to position the chromophores.¹³ Self-assembled systems of dye molecules are much easier to mimic in laboratories than structures prepared by careful positioning using proteins.^{4,14,15}

Chlorosomes are elongated organelles that contain several tens of self-assembled supramolecular aggregates, each composed of thousands of BChl c, d, and e molecules.^{16–22} The supramolecular organization of BChl molecules in these aggregates, which is of crucial importance for the light-harvesting efficiency, is still a subject of ongoing debate. Many previous studies have led to the proposal of tubular, lamellar, and rolled lamellar structures for the self-assembled aggregates.^{6,13,22–29} These shapes and the molecular packing in the aggregates have been obtained through the combined use of mutagenesis, solid-state nuclear magnetic resonance (NMR), cryogenic electron microscopy (Cryo-EM),

single chlorosome linear polarization resolved fluorescence excitation spectroscopic studies, and molecular modeling.^{6,24–26,30,31} The debates about the exact structure may be explained from the fact that the aggregate formation depends on the bacterial strain used and the precise growth conditions. Moreover, the hierarchical structure is prone to heterogeneity, which complicates finding a unique organization. First, structural disorder occurs inside each aggregate because different BChl molecules (c, d, and e), each of which can further vary in their state of methylation, are randomly used in the aggregation process. Second, variations in size of the aggregates may occur within and between individual chlorosomes.

In this study, we investigate theoretically to what extent size variation of the constituent BChl aggregates in different chlorosomes can be probed using single-chlorosome spectroscopy. We adopt the picture that the dominant secondary structural elements inside the chlorosomes are tubular aggregates, which may differ in radius and length. It is known from previous studies that the optical and energy transport properties of (tubular) aggregates not only depend on the molecular packing (intermolecular distances and orientations)^{15,32–36} but may also depend on the aggregate radius and the length. In particular, the isotropic absorption and linear dichroism (LD) spectra of tubular aggregates were shown to depend on the radius,^{32,37,38} while it has been suggested that the circular dichroism spectrum of tubular aggregates is sensitive to their length up to rather long lengths.^{39–41} Furthermore, the exciton diffusion constant is sensitive to the ratio of the exciton delocalization length and the radius,⁴² where the delocalization length itself also shows a dependence on both the radius and the length.⁴³ All this makes it of interest to investigate how variations in the radius and length of tubular aggregates in different chlorosomes influence light-harvesting properties and whether such variations may be probed experimentally.

To study variations between chlorosomes, the application of single-molecule spectroscopy is indispensable.^{44–47} Since chlorosomes contain many thousands of molecules, we rather refer to the application of this type of spectroscopy to chlorosomes as single-object spectroscopy. Prior studies have applied single-object linear polarization (SOLP) resolved fluorescence excitation spectroscopy to individual chlorosomes, in which fluorescence excitation spectra for different linear polarization directions of the exciting light are recorded; hereafter, we refer to this as SOLP spectroscopy. SOLP spectroscopy gives much more information than LD spectroscopy, which measures the difference in the absorption spectra for two perpendicular polarization directions on an ensemble of oriented objects (molecules, aggregates, and nanostructures).⁴⁸ The SOLP studies of chlorosomes from the wild-type and two mutant species of *Chlorobaculum tepidum* were consistent with a tubular geometry of the BChl aggregates for the mutants and the majority of the wild-type chlorosomes.^{30,49} They showed an energy difference between two mutually perpendicular exciton transitions in tubular aggregates, which varied between different chlorosomes. Inspired by earlier work,³² these variations were interpreted in terms of variations in the average radii of the tubular aggregates in different chlorosomes.⁴⁹ In these studies, a possible length variation of the aggregates was not considered, as the length generally has a much more limited effect on the linear-polarization dependent spectroscopy of tubular aggregates.^{39,43}

Motivated by previous reports that circular dichroism (CD) spectroscopy may show an interesting and prolonged dependence on the length of tubular aggregates,^{39–41} this study investigates whether single-object CD spectroscopy (SOCD spectroscopy), in combination with SOLP spectroscopy, may be sensitive to variations in (average) length as well as (average) radius of the constituent tubular aggregates between different chlorosomes. Many CD studies have been reported on ensembles of chlorosomes,^{13,50–55} but thus far only one study has reported CD spectra of single chlorosomes, and in that case, the CD strength was only measured at one frequency.⁵⁶ More generally, SOCD studies are scarce, although some results have been reported for single molecules^{57–60} and others for individual nano-structures,^{61–63} showing that, in principle, the sensitivity required for SOCD spectroscopy can be achieved. To the best of our knowledge, the theory of SOCD spectroscopy was not developed.

We first study the simplest situation, assuming that the radius of the tubular aggregates is the same for all aggregates in all chlorosomes. For definiteness, we use the average radius derived from SOLP experiments on chlorosomes of the bchR mutant of *Chlorobaculum tepidum*;⁴⁹ in addition, the molecular packing derived in that study is used as the basis for our model calculations. We model SOCD as well as SOLP spectra for this situation. From this, we find that the SOCD spectra may indeed probe differences in aggregate length between individual chlorosomes. Ideally, the experiment should measure these spectra as a function of the angle between the wave vector of the exciting light and the tubular axes; if variation of this angle is not possible, the optimal setup is to use 45° for this angle. We observe that these findings are still valid even when we allow for a distribution of aggregate lengths within individual chlorosomes. In that case, SOCD spectroscopy is able to probe differences in the average aggregate length realized for different chlorosomes because the shape of the spectrum turns out to be sensitive to the average length. We also show that the shape of the SOLP spectra has a much weaker length dependence, making it very hard to retrieve length information from SOLP spectroscopy alone.

In the next step of our study, we allow for variations in length as well as radius of the aggregates between chlorosomes. We find that, generally, it is not possible to retrieve the aggregate radius that applies to a particular chlorosome uniquely from SOLP experiments because the energy difference between the two mutually perpendicular transitions also turns out to depend on the aggregate length. However, our results show that for a given value of this energy separation, the combination of SOLP and SOCD spectroscopy, together with spectral modeling, gives sufficient information to probe what combination of length and radius applies to the aggregates within a particular chlorosome. Like in the first part of our study, we show that this conclusion still holds for the more realistic situation where the length and the radius of ~50 aggregates within a chlorosome do not all have the same value but are taken randomly from particular distributions. In that case, the combination of SOLP and SOCD spectroscopies, together with spectral modeling, allows one to extract the average length and average radius of the tubular aggregates within an individual chlorosome.

The outline of the remainder of this paper is as follows: In Sec. II, we first describe the structural model and the Frenkel exciton model used to calculate the SOLP and SOCD spectra of chlorosomes.

Next, in Sec. III, numerical results are presented and discussed, first for the case where we assume the same radius for all tubular aggregates, followed by a detailed study of the case where both lengths and radii of the aggregates are allowed to vary. Finally, we conclude in Sec. IV.

II. MODEL

A. Tubular aggregate structure

The model structure we used for the tubular aggregates in chlorosomes of *Chlorobaculum tepidum* is identical to the one found in Ref. 49 by using SOLP spectroscopy in combination with earlier results.²⁶ The model is constructed as depicted in Fig. 1. We start from a two-dimensional lattice with two molecules per unit cell (indicated by green and red arrows, see below for more detail), as depicted in Figs. 1(a) and 1(b) (the latter indicating a side-view looking along the a -axis). The lattice constants are given by $a = 1.25$ nm and $b = 0.98$ nm, and the angle between both lattice directions is $\gamma = 122^\circ$. This lattice is rolled onto a cylindrical surface along the rolling vector \mathbf{C} that connects two lattice points. This vector is determined by its length $|\mathbf{C}| = 2\pi R$ and its angle relative to the a -axis, denoted as δ [see Fig. 1(a)]. Following Ref. 49, we use $\delta = 70^\circ$. This wrapping results in a tubular aggregate of radius R (taking discrete values only), with two molecules per unit cell [Fig. 1(c)]. The aggregate has a helical structure due to the angle δ differing from 0° and $(180^\circ - \gamma) = 58^\circ$. It can be seen alternatively as a perpendicular stack of N_1 rings, where each ring contains the centers of N_2 equidistant unit cells.³² Neighboring rings are separated by a distance $h = 0.11$ nm (dictated by δ and the lattice constants) and are rotated relative to each other over an angle ζ , which also depends on R (or N_2).

The two molecules in each unit cell are positioned in a symmetric way along the a -axis and only differ in their orientations relative

to the lattice plane, ultimately resulting in the farnesyl tails of the BChl molecules pointing alternately in and out of the cylindrical surface: syn-anti stacking.²⁶ For the optical properties, it is important to characterize the relevant molecular transition dipoles (see Sec. II B). In Fig. 1, these dipoles are indicated by the green and red arrows, whose projections on the plane of the lattice make an angle of $\eta = 35^\circ$ with the a -axis; their angles with the lattice plane alternate for the syn- and the anti-orientations and take the values $\pm\alpha = \pm 4^\circ$ [Fig. 1(b)].

For each choice of R , the above procedure and parameters uniquely specify the positions of all molecules inside the aggregate and the orientations of their dipoles. This, in turn, uniquely defines the exciton Hamiltonian that allows us to calculate the optical properties (Sec. II B). As explained in the Introduction, in the first part of this study, we will assume that R is the same for all tubular aggregates in all chlorosomes. To be specific, we will use the value $R = 15.42$ nm, which is the discrete value allowed by the lattice parameters that is closest to the average value of about 15 nm found from the analysis of the SOLP studies on the bchR mutant of *Chlorobaculum tepidum* in Ref. 49. This model corresponds to $N_2 = 10$. In the second part of our study, where we allow R to vary, it takes discrete values $R = N_2 \times 1.542$ nm, where we vary N_2 in the range $N_2 = 1, \dots, 35$, which covers the entire distribution of values found in Ref. 49.

B. Frenkel exciton model and spectra

To calculate the optical properties of the tubular aggregates inside the chlorosomes, we use the Frenkel exciton model that accounts for the Q_y excitation on each BChl molecule and the excitations transfer interactions between each pair of molecules,

$$H = \sum_{n,m} H_{nm} |n\rangle \langle m| = \sum_n E_{\text{mol}} |n\rangle \langle n| + \sum_{n,m \neq n} V_{nm} |n\rangle \langle m|. \quad (1)$$

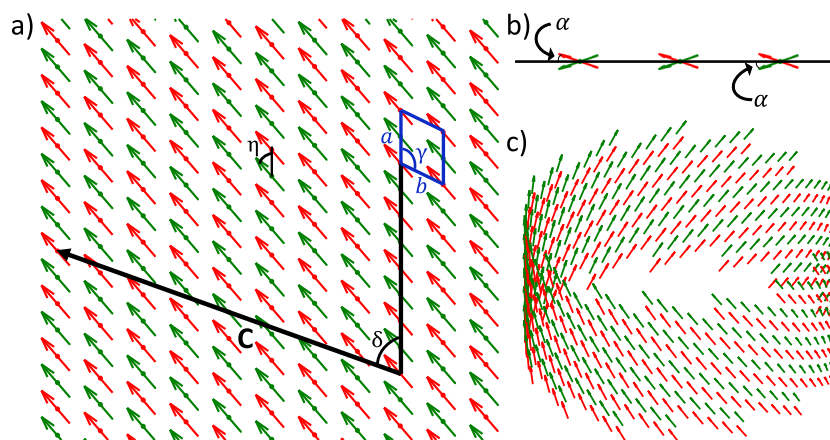


FIG. 1. Construction of the model structure of the tubular arrangement of the BChl molecules. The starting point is a planar lattice with two molecules per unit cell [panel (a); the unit cell is indicated in blue], only differing in their orientation relative to the lattice plane [panel (b) for side-view along the a -axis]. This lattice is wrapped over the rolling vector \mathbf{C} , making an angle δ with the a -axis, onto a cylindrical surface with radius R to define the helical tubular structure [panel (c)], where all molecular positions are uniquely defined in terms of the lattice constants (a , b , and γ), the radius R , and the angle δ . The red and green arrows indicate the dipoles of the relevant optical transition (the Q_y transition) in each molecule. Their projections on the lattice plane make an angle η with the a -axis and an alternating angle of $\pm\alpha = \pm 4^\circ$ with the lattice plane. The parameters we used in our calculations were⁴⁹ $a = 1.25$ nm, $b = 0.98$ nm, $\gamma = 122^\circ$, $\delta = 70^\circ$, and $\eta = 35^\circ$. The radius R can take a discrete set of values, depending on the model situation considered.

Here, $|n\rangle$ is the state with molecule n excited and all other molecules in their ground state, E_{mol} indicates the energy of the molecular Q_y excitation, and V_{nm} is the excitation transfer interaction between molecules n and m . We will ignore energy and interaction disorder, focusing totally on the effects of aggregate length and radius on the spectra. This leads to exciton eigenstates of the Hamiltonian that are fully delocalized over the tubular aggregate. Models including disorder in tubular aggregates have shown that localization is rather weak in these systems;^{43,64} moreover, the results of SOLP spectroscopy on chlorosomes indeed reflect strongly delocalized states.^{30,49} For the monomer excitation energy, we use $E_{\text{mol}} = 15\,931.4\text{ cm}^{-1}$, which gives a good fit to the experimental ensemble CD spectrum of bChR, shown in Fig. S1 in the [supplementary material](#) (Note 1).⁶⁵ The interactions V_{nm} were modeled using a point-dipole approximation,

$$V_{nm} = \frac{\boldsymbol{\mu}_n \cdot \boldsymbol{\mu}_m}{r_{nm}^3} - 3 \frac{(\boldsymbol{\mu}_n \cdot \mathbf{r}_{nm})(\boldsymbol{\mu}_m \cdot \mathbf{r}_{nm})}{r_{nm}^5}, \quad (2)$$

where $\boldsymbol{\mu}_n$ is the transition dipole vector of molecule n , \mathbf{r}_{nm} indicates the position vector between molecules n and m , and r_{nm} is its magnitude. (Model calculations using interactions between extended dipoles do not change our conclusions; they hardly affect the spectral lineshapes and mostly show an overall shift.) Using the structural data in Sec. II A together with the value $\mu = 5.5\text{ D}$ for the magnitude of the dipole of the Q_y transition,^{26,30} all interactions can be calculated and the collective eigenstates can be obtained through numerical diagonalization of the matrix H_{nm} as

$$|k\rangle = \sum_n \varphi_{kn} |n\rangle, \quad (3)$$

where φ_{kn} denotes the n th component of the k th eigenvector of H_{nm} ; the corresponding eigenenergy is denoted as E_k .

From the exciton states, the SOLP and SOCD spectra for the tubular aggregates can be obtained (see below). We must keep in mind that ultimately we are interested in the spectra for chlorosomes, which consist of several tens of aggregates. When modeling the chlorosome spectra, we will assume that the interactions between individual tubes within a chlorosome are weak enough to be ignored, which implies that the optical properties are determined by the (averaged) optical properties of the individual aggregates that make up a chlorosome. This is corroborated by the fact that previous experiments have been well understood on the basis of this assumption.⁴⁹

Furthermore, to calculate the various polarization dependent spectra of chlorosomes, we assume that the tubular aggregates within an individual chlorosome are all aligned, which results in a common axis, referred to as the tubular axis of the chlorosome. Cryo-EM micrographs of isolated chlorosomes from *Chlorobaculum tepidum* and its mutants in amorphous ice show striated lines in the side-on view and circular ring structures from the end-on view.^{6,26,27} This suggests that tubular aggregates inside chlorosomes are indeed aligned and are oriented with their axes parallel to the long axis of the chlorosome they reside in. Single-chlorosome experiments are carried out on chlorosomes adsorbed on a substrate. Using atomic force microscope (AFM) and linear dichroism (LD) studies,^{45,66} it has been shown that the long axes of the chlorosomes lie parallel to the plane of the substrate (this orientation can be steered using various methods, such as enclosing the chlorosomes in a gel and squeezing

the gel along a particular direction^{50,51,67–70}). We therefore assume that the axes of the tubular aggregates inside the chlorosomes are all parallel to the experimental substrate. This is further supported by the results of SOLP measurements, where experimental spectra also strongly suggest this orientation.^{30,49}

The above allows us to focus on the calculation of spectra of individual tubular aggregates with their long axes mutually aligned and parallel to the experimental substrate. We first turn our attention to SOLP spectroscopy, single-chlorosome fluorescence excitation spectroscopy using linearly polarized light (see Fig. 2). In this experiment, light is incident from above, perpendicular to the substrate. The experiment is performed by measuring the dependence of the fluorescence excitation spectrum on the angle ϕ of the polarization direction of the light relative to a reference direction on the substrate, for which we may choose, without loss of generality, the direction of \mathbf{T} . We remind the reader that the single-object fluorescence excitation spectrum is the emission intensity of the object as a function of the frequency (energy) of the exciting photons. Here, the emission is usually from the relaxed state and assuming that the fluorescence quantum yield does not depend on the excitation frequency, as is commonly done, this spectrum is identical in shape to the absorption spectrum. For this reason, the SOLP and SOCD spectra in this study have all been calculated as absorption spectra.

Thus, in terms of the exciton eigenstates and energies, the SOLP spectrum of a single aggregate may be expressed as

$$A_e(E) = \frac{1}{\pi} \sum_k |\boldsymbol{\mu}_k \cdot \mathbf{e}|^2 \frac{\Gamma_k}{(E - E_k)^2 + \Gamma_k^2}, \quad (4)$$

with E being the photon energy of the exciting light, $\boldsymbol{\mu}_k = \sum_n \varphi_{kn} \boldsymbol{\mu}_n$ being the transition dipole from the aggregate's ground state to the exciton state k , \mathbf{e} being the unit vector indicating the orientation of the polarization of the light, and Γ_k being the dephasing rate of the k th exciton transition. Obviously, the spectra $A_{\parallel}(E)$ and $A_{\perp}(E)$, obtained for \mathbf{e} parallel ($\phi = 0^\circ$) and perpendicular ($\phi = 90^\circ$) to the tubular axis, are natural basic spectra, from which the spectra for all other polarizations \mathbf{e} are easily obtained,

$$A_e(E) = A_{\parallel}(E) \cos^2 \phi + A_{\perp}(E) \sin^2 \phi. \quad (5)$$

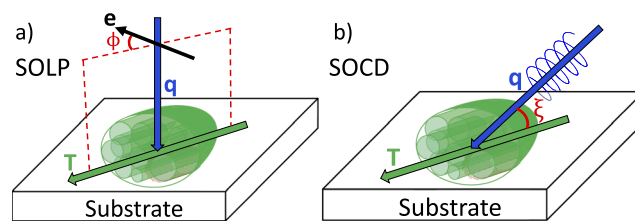


FIG. 2. Setup for single-chlorosome fluorescence excitation spectroscopy using (a) linearly polarized light (SOLP spectroscopy) and (b) circularly polarized light (SOCD spectroscopy). The chlorosome lies on the substrate with its tubular axis \mathbf{T} (parallel to the tubular axes of its constituent molecular aggregates) oriented parallel to the plane of the substrate. For SOLP spectroscopy, linearly polarized light with wave vector \mathbf{q} (blue arrow) is incident perpendicular to the substrate; its polarization vector \mathbf{e} makes an angle ϕ relative to \mathbf{T} . For SOCD spectroscopy, the wave vector \mathbf{q} of circularly polarized light (blue spirals) makes an angle ξ with \mathbf{T} .

Owing to the cylindrical symmetry, tubular aggregates only have exciton transitions with transition dipole either exactly parallel or exactly perpendicular to the tubular axis.^{39,41} The ratio of the total oscillator strengths in both directions is determined by the angle β between the molecular transition dipoles and the tube's axis, which from the parameters in Sec. II A is found to be $\beta = 90^\circ - \delta + \eta = 55^\circ$ (ignoring minor corrections resulting from the small angle $\pm\alpha$). In the situation considered here, with light incident perpendicular to the tube's axis, only half of the perpendicular oscillator strength contributes to the spectrum with \mathbf{e} perpendicular to the cylinder axis: $O_{\parallel}/O_{\perp} = 2 \cot^2 \beta$, with O_{\parallel} (O_{\perp}) being the integrated spectrum for \mathbf{e} parallel (perpendicular) to the tube's axis. For general reference, we also define the single-chlorosome LD spectrum as

$$LD(E) = A_{\parallel}(E) - A_{\perp}(E). \quad (6)$$

Next, we turn our attention to the CD spectrum, which is defined as the difference between the absorption spectrum of left (L) and right (R) circularly polarized light,

$$CD(E) = A_L(E) - A_R(E). \quad (7)$$

In conventional CD spectroscopy, the spectra are measured in an isotropic ensemble; previous expressions for the CD spectrum of chlorosomes indeed have been derived taking an isotropic average over all possible orientations of the tubular axis of the chlorosomal molecular aggregates.^{39,40} In the case of single-chlorosome CD spectroscopy, such an average does not apply: the exciting light then has a well-defined, unique direction of incidence relative to the tubular axis and the choice of this direction has a strong influence on the resulting spectrum, as we will see. In contrast to SOLP spectroscopy, where light incident perpendicular to the substrate provides us with all important information, we will see that perpendicular incidence is not optimal for getting most information out of SOCD spectroscopy. For this reason, we start by allowing for the most general situation (owing to the cylindrical symmetry), where the wave vector \mathbf{q} of the circularly polarized light makes an arbitrary angle ξ with the tubular axis of the chlorosome (see Fig. 2).

The CD spectrum for a single tubular aggregate may be derived using Fermi's golden rule to account for the interaction between the circularly polarized light and the aggregate, similar to the standard derivation of the ensemble averaged CD.^{1,39,71} The resulting spectrum for light incident with wave vector \mathbf{q} reads

$$CD_{\mathbf{q}}(E) = \frac{1}{\pi} \sum_k R_k^{\mathbf{q}} \frac{\Gamma_k}{(E - E_k)^2 + \Gamma_k^2}, \quad (8)$$

where E , E_k , and Γ_k are as defined above and the rotational strength equals^{69,70}

$$R_k^{\mathbf{q}} = \frac{\lambda}{8\pi} \sum_{n,m} \varphi_{kn} \varphi_{km}^* \sin(\mathbf{q} \cdot \mathbf{r}_{nm}) [\mathbf{q} \cdot (\boldsymbol{\mu}_n \times \boldsymbol{\mu}_m)], \quad (9)$$

where λ is the wavelength of the incident light and the quantities φ_{kn} , \mathbf{r}_{nm} , and $\boldsymbol{\mu}_n$ are as defined above. For aggregate sizes (lengths and radii) small compared to an optical wavelength, the expression $\sin(\mathbf{q} \cdot \mathbf{r}_{nm})$ may be linearized, which allows for a faster numerical implementation. In practice, we have used this linearization in

all numerical spectra reported here. We have checked that even for lengths as long as 200 nm, this has a negligible effect on the shape of the SOCD spectra (see Note 2 of the [supplementary material](#)).

It can be shown (see Note 3 of the [supplementary material](#)) that like in the case of SOLP spectroscopy, also for SOCD spectroscopy in the long-wavelength limit, where $\sin(\mathbf{q} \cdot \mathbf{r}_{nm})$ in Eq. (9) is linearized, a decomposition in two basic spectra is possible,

$$CD_{\mathbf{q}}(E) = CD_{\xi}(E) = CD_{\parallel}(E) \cos^2 \xi + CD_{\perp}(E) \sin^2 \xi, \quad (10)$$

where $CD_{\parallel}(E)$ is the spectrum for $\xi = 0^\circ$ (which in experiment cannot be achieved fully due to the substrate) and $CD_{\perp}(E)$ is the spectrum for $\xi = 90^\circ$. The first equality in Eq. (10) holds due to the rotational symmetry of the tubular aggregates. Because the long-wavelength limit holds for aggregates as long as 200 nm, which covers the maximum lengths expected in chlorosomes, the decomposition [Eq. (10)] holds for chlorosomes. This decomposition could open the way to SOCD spectroscopy where ξ is scanned over a maximum range, improving the signal-to-noise ratio to obtain the two basic spectra in a global fit, similar to applications of SOLP spectroscopy where ϕ is scanned.^{30,35,49} As we will see, however, even the application of SOCD spectroscopy with one well-chosen value of ξ provides much information.

C. Selection rules and basic spectral features

In this subsection, we address general features of the SOLP and SOCD spectra for tubular aggregates that can be obtained (semi-)analytically. To this end, we consider the limit of long tubular aggregates, where the exciton states can be obtained analytically by imposing periodic boundary conditions along the tube's axis. The exciton states then take the form of Bloch waves in both the axis direction (owing to the boundary conditions) and the ring direction (owing to the cylindrical symmetry), with quasimomenta $2\pi k_1/N_1$ and $2\pi k_2/N_2$, respectively, with k_1 and k_2 integers. This leads to strong optical selection rules on the vector $\mathbf{k} = (k_1, k_2)$, which replaces the scalar label for the exciton eigenstates (k) in Eqs. (4) and (8): only states with $\mathbf{k} = (0, 0)$ and $\mathbf{k} = \pm \mathbf{h}$ with $\mathbf{h} = (N_1 \zeta / 2\pi, 1)$ contribute to the spectra.³⁹ These are known as super-radiant states with oscillator strengths and rotational strengths that scale proportional to the total number of molecules in the tube. For the case of tubular aggregates with one molecule per unit cell, this leads to three super-radiant states, where the totally symmetric one ($\mathbf{k} = \mathbf{0}$) has a transition dipole of magnitude $\sqrt{N_1 N_2} \mu \cos \beta$, directed parallel to the tube's axis, while the two "helical" states $\mathbf{k} = \pm \mathbf{h}$ are degenerate and have dipoles of magnitude $\sqrt{N_1 N_2} / 2 \mu \sin \beta$, both perpendicular to the axis and perpendicular to each other.³⁹ For the SOLP spectra, this implies that both $A_{\parallel}(E)$ and $A_{\perp}(E)$ have one peak, positioned at the eigenenergies E_0 and E_h , respectively (see Note 4 of the [supplementary material](#) for more details).

The structure considered here has two molecules per unit cell, which only differ from each other in the small tilt angle $\pm\alpha$ of the dipoles. While the numerical calculations reported in Sec. III were all done including this dimerization, properly accounting for having a Davydov splitting, this induces only minute corrections in the spectrum to the approximation where we set $\alpha = 0^\circ$. Therefore, the calculated spectra are well understood using a one-molecule per unit cell picture, which for long tubes thus leads to one peak in both

$A_{\parallel}(E)$ and $A_{\perp}(E)$. For the structure considered here, the parallel transition has lower energy than the perpendicular one ($E_0 < E_h$). This allows one to find the orientation of the tube (chlorosome) on the substrate by recording the spectrum as a function of the polarization angle ϕ . For short tubes, finite-size effects will lead to small shifts of both peaks. Moreover, the periodic boundary conditions in the axis direction then are no longer valid, breaking the selection rules on k_1 . This leads to weak satellite peaks, which are blue shifted compared to the main peaks. Details on the effects of dimerization and finite length are analyzed in the [supplementary material](#) (Note 4).

The CD spectrum for an isotropic ensemble of long tubular aggregates with one molecule per unit cell was analyzed in Ref. 39. There, a distinction was made between “ring” and “helical” contributions to this spectrum. Interestingly, for the case of SOCD spectroscopy, $CD_{\parallel}(E)$ is totally determined by helical contributions, while $CD_{\perp}(E)$ only has ring contributions. For the structure considered here (ignoring effects of a Davydov splitting), negative ring contributions occur at $E = E_0$, while positive ring contributions occur at $E = E_h$, leading to an overall dispersive (S-type) spectral shape centered between E_0 and E_h . Two degenerate dispersive helical contributions are centered at $E = E_h$; they are derivatives of Lorentzian lineshapes, i.e., they also give an S-type shape, but in this case with the positive part on the low-energy side and the negative part toward higher energies. All these notions survive if we take into account the dimerization due to the small angle $\pm\alpha$ (see Note 5 of the [supplementary material](#)): one Davydov component dominates the entire spectrum and the spectral contributions arising from the second (higher-energy) Davydov band can be ignored in practice; a new type of contribution arising from the dimerization, namely, a non-dispersive helical contribution in both Davydov bands, is so small, in practice, that it can also be ignored.

From the above, we see that for general ξ , the sum of two partially overlapping S-type lineshapes of the opposite overall sign determine the SOCD spectrum. This makes the spectrum highly sensitive to ξ , to the precise values of the energies E_0 and E_h of the super-radiant exciton states (which depend on the aggregate radius and length), and to the relative magnitude of both dispersive shapes. The latter depends on the length: at small length, both are similar in magnitude, but for increasing length, the helical contributions become more important. It is this sensitivity, which will be confirmed in the numerical results in Sec. III, that allows for probing the radius and length using the combination of SOLP and SOCD spectroscopies.

III. NUMERICAL RESULTS AND DISCUSSION

In this section, we present the results of our model calculations for the single-chlorosome spectra as a function of linear polarization of the exciting light (SOLP) and the single-chlorosome CD spectra. As explained in Sec. II, we calculate the spectra as the average of the spectra of the individual tubular BChl aggregates that make up the chlorosome and assume that all tubular axes inside a chlorosome are aligned and parallel to the experimental substrate (see Fig. 2). The model for each tube is constructed as specified in Sec. II A, with model parameters indicated in Fig. 1 and their values specified in its caption. These parameters are fixed for all calculations performed. The lengths L and the radius R of the tubular aggregates,

alternatively represented as N_1 ($L = N_1 \times 0.11$ nm) and N_2 ($R = N_2 \times 1.542$ nm) of the cylinders, may differ and will be specified below for the different cases considered. The parameters that further define the Hamiltonian are given in Sec. II B; specifically, we have $E_{\text{mol}} = 15\,931.4$ cm⁻¹ for the molecular excitation energy and we use dipole-dipole excitation transfer interactions, with a dipole strength of $\mu = 5.5$ D and orientations as given in Fig. 1. Finally, we use $\Gamma_k = 50$ cm⁻¹ for the exciton dephasing rate. This parameter is not known experimentally; from two-dimensional spectroscopy at zero waiting time, an upper bound of 180 cm⁻¹ can be deduced.⁷² All numerical calculations were performed with open boundary conditions in the axis direction of the tubes.

A. Model with fixed tubular radii

As explained in the Introduction and Sec. II A, we first analyze spectra in case all tubular aggregates in all chlorosomes have the same radius of $R = 15.42$ nm ($N_2 = 10$). In the simplest approach, we will assume that all tubes inside one chlorosomes have equal length L and that this parameter may vary between chlorosomes. In this case, the SOLP and SOCD spectra of a single chlorosome are simply given by the spectra for a single tube of length L .

Figure 3 presents as contour plots the calculated SOCD spectra for chlorosomes consisting of tubular aggregates with eight different lengths L (constant within each chlorosome) as a function of the angle ξ . As we argued in Sec. II B, SOLP spectroscopy allows one to assess the orientation of the tubular axis for a single chlorosome, which, in practice, may serve as reference for determining the angle ξ in an SOCD experiment. It is clearly seen that indeed the SOCD spectrum depends on ξ as well as L ; we have checked numerically that for every angle, the spectrum indeed can be obtained through a linear combination of the spectra for $\xi = 0^\circ$ and $\xi = 90^\circ$ [Eq. (10)]. These two basic spectra indeed follow the general description given in Sec. II C. For the longest tubes, the spectrum at $\xi = 0^\circ$ shows a dispersive shape centered at $E = E_h < E_{\text{mol}}$, deriving from the helical exciton state (helical contribution), while the spectrum at $\xi = 90^\circ$ shows a dispersive shape centered at slightly lower energies (namely, in between E_0 and E_h) and with sign swapped relative to the spectrum at $\xi = 0^\circ$ (the ring contribution). When the length gets shorter, we indeed observe overall shifts in both features and the separation between positive and negative peaks grows. Moreover, for the shortest lengths (5 and 10 nm), we see additional peaks appearing on the higher-energy side of the main features due to finite size effects. Finally, we note that for the longest tubes, the helical contribution is larger than the ring contribution; for short tubes, they are roughly equally strong.

For angles ξ in between 0° and 90° , the linear combination of both basic spectra gives rise to a richer variation of lineshapes, with the possibility to have more than one sign change as a function of E . As a consequence, at such intermediate angles, the spectrum is more sensitive to L than at $\xi = 0^\circ$ and $\xi = 90^\circ$ and the L dependence persists for larger L values (up to about 50 nm). This is seen more clearly by making cuts through the contour plots, which are shown in Fig. 4 for five different angles ξ (0° , 30° , 45° , 60° , and 90°), each for six different values of L . These plots show that, in particular, the structure of the spectrum varies much more as a function of length for $\xi = 45^\circ$ as compared to other angles, which makes this angle of incidence the most sensitive one to probe length variations. We can also

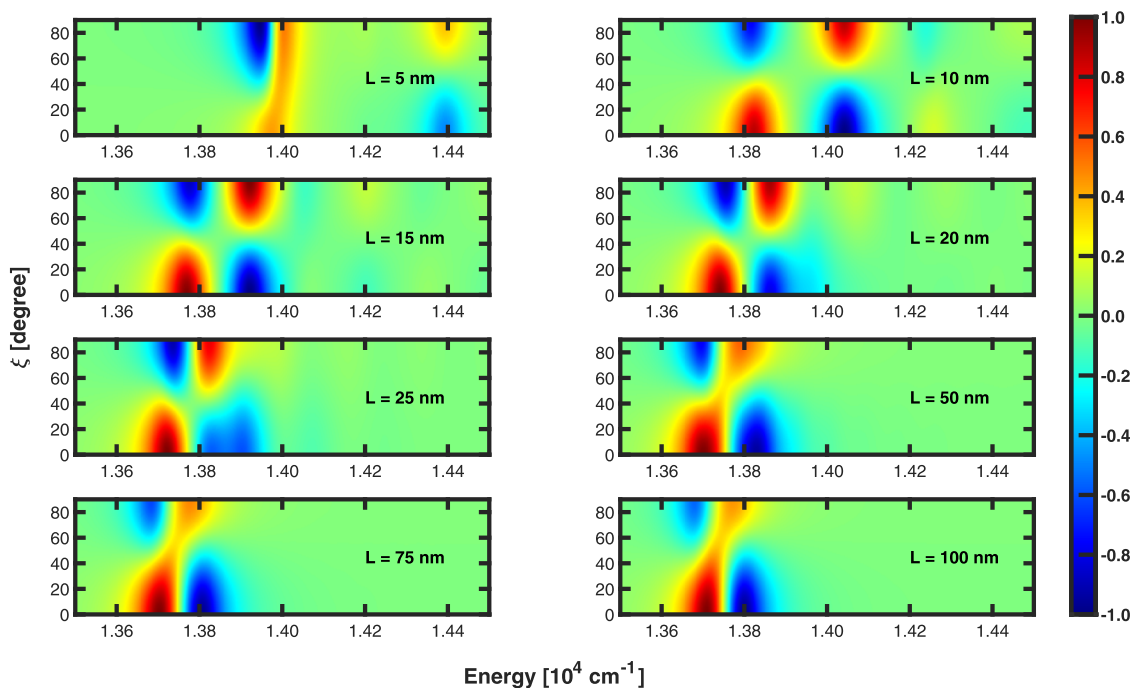


FIG. 3. Contour plots that present single-chlorosome CD spectra as a function of excitation energy and angle ξ between the wave vector \mathbf{q} of the incident light and the chlorosome's tubular axis. Each panel corresponds to a chlorosome with different length L of the tubular BChl aggregates it consists of, as specified in the panel. All tubes within one chlorosome have the same length; all aggregates have the same radius of $R = 15.42$ nm. The spectrum in each panel is normalized to its maximum absolute intensity.

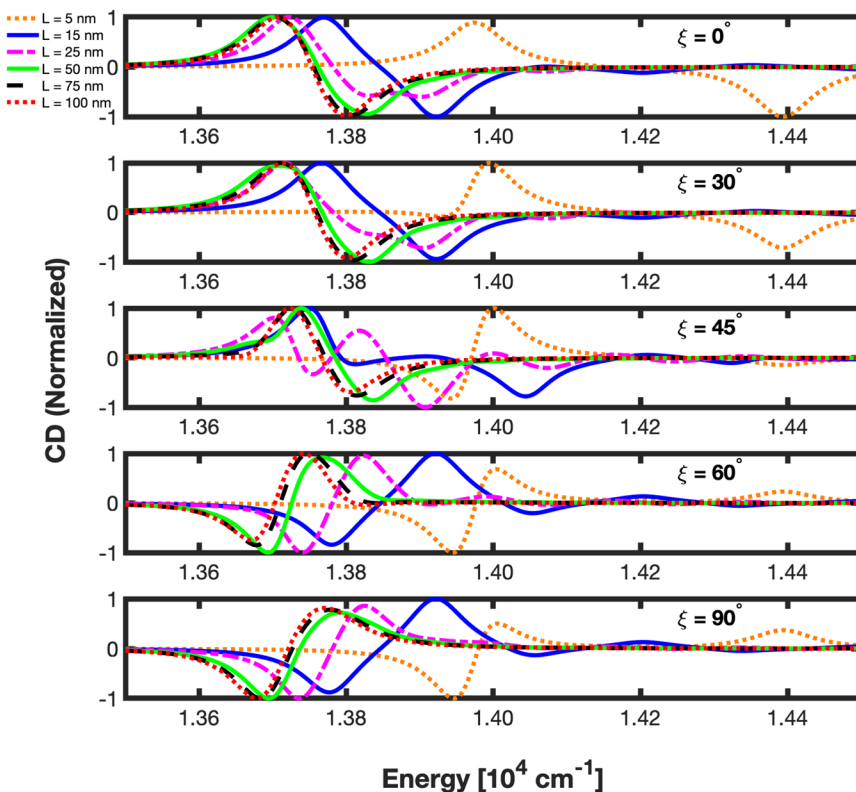


FIG. 4. Cross sections through the contour plots of Fig. 3. Each panel presents the cross sections for six different values of the aggregate length L , coded as specified next to the first panel, for a specific angle ξ , as indicated inside the panels. Each spectrum is normalized to its maximum absolute intensity.

conclude that the typical experimental setup used for single-object spectroscopy, where light is incident perpendicular to the substrate, is not optimal for using SOCD spectroscopy to measure length variations in chlorosomes. The ideal would be to measure the complete contour plot, as this would give most information, but if the experimental setup dictates that only one angle can be used, clearly $\xi = 45^\circ$ seems the best choice. The crux is that at this angle, there is a large contribution from both the ring and the helical spectra, whose interference depends on the length L due to the fact that the relative magnitude of both spectra depends on L .

Thus far, we considered the situation where the tubular aggregates inside a chlorosome all have the same length. This makes the distinction between different chlorosomes sharp and enhances the possibility to probe the (typical) length of the aggregates they consist of. To see whether some amount of length variation within individual chlorosomes washes out the spectral details that reflect the typical aggregate length, we extend the previous model by allowing for such variations. Individual chlorosomes are known to contain

several tens of molecular aggregates.^{1,2} In our model, we assume that each chlorosome contains 50 tubular molecular aggregates, which are identical in all aspects (also radius), apart from their length. The lengths are chosen randomly from a Poisson distribution with average \bar{L} .⁷³ The advantage is that this is a simple one-parameter distribution, whose variance is equal to its average; this implies that at later stages of the growth of the aggregates inside a chlorosome, the absolute variation in their sizes also grows, which seems a natural assumption to make. Thus, each individual chlorosome is specified by 50 randomly chosen values of L using as a starting point a specific average \bar{L} . This leads to chlorosomes with a random distribution of aggregate lengths; each individual chlorosome may be characterized by the average length of its aggregates (\bar{L}) (not necessarily equal to \bar{L}). The SOLP and SOCD spectra for an individual chlorosome are then obtained by adding the corresponding spectra of the 50 constituent tubular aggregates (properly accounting for the fact that longer aggregates have a larger weight in the spectrum).

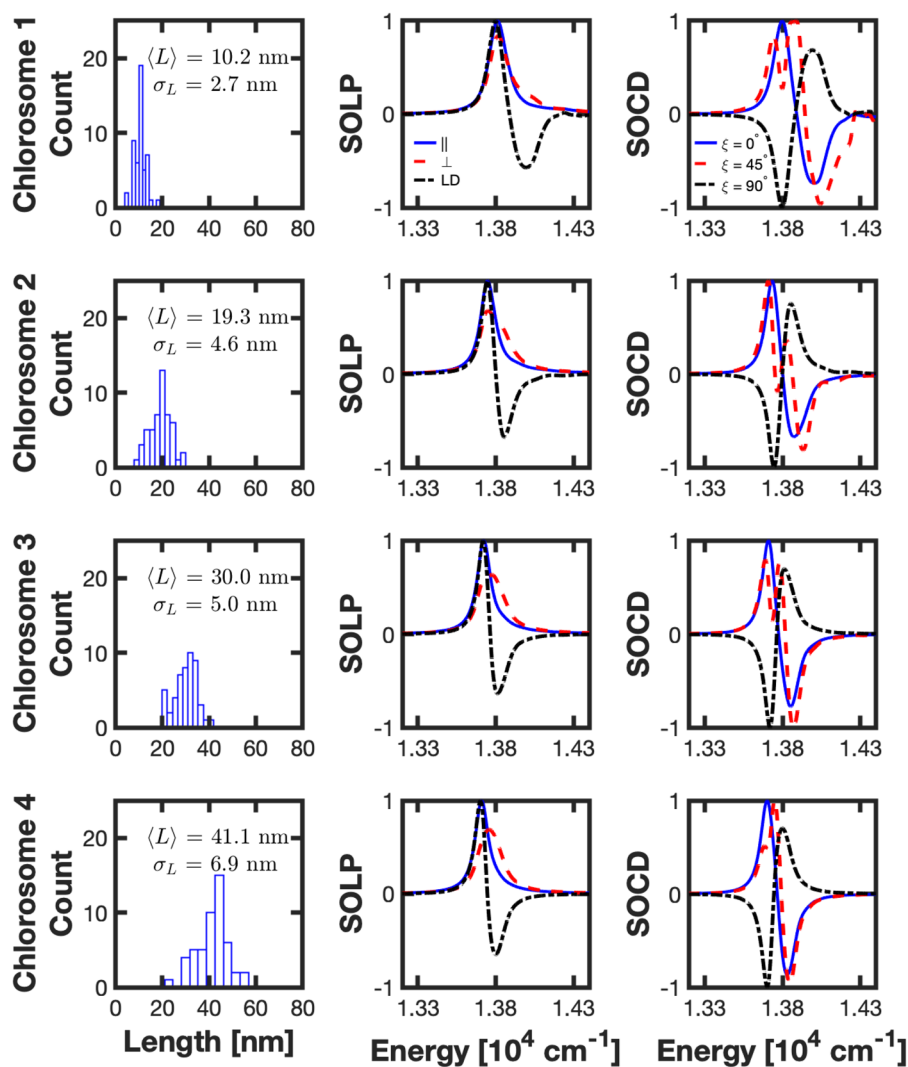


FIG. 5. Left column: histograms for the occurrence of the length of the 50 tubular aggregates in four randomly generated chlorosomes using the Poisson distributions for L with four different averages \bar{L} (10, 20, 30, and 40 nm from top to bottom), with mean $\langle L \rangle$ and standard deviation σ_L of each histogram as indicated. The radii of all tubular aggregates in the chlorosomes are taken equal, $R = 15.42$ nm. Middle column: SOLP spectra calculated for these individual chlorosomes, with light polarized parallel [$A_{\parallel}(E)$, blue solid line] and perpendicular [$A_{\perp}(E)$, red dashed line] to the tubular axis; the black dashed-dotted line shows the single-chlorosome LD spectrum. $A_{\parallel}(E)$ and $A_{\perp}(E)$ are normalized to the largest one of the peak intensities of the two; each LD spectrum is normalized to its maximum absolute intensity. Right column: SOCD spectra $CD_{\xi}(E)$ calculated for these individual chlorosomes for three angles between the direction of incidence of the light and the chlorosome's tubular axis: $\xi = 0^\circ$ (solid blue line), 45° (red dashed line), and 90° (black dashed-dotted line). Each CD spectrum is normalized to its maximum absolute intensity.

Figure 5 shows the results for four particular chlorosomes generated from Poisson distributions with four different values of \bar{L} , namely, 10, 20, 30, and 40 nm, from top to bottom, respectively. The left column presents the histograms for the aggregate lengths found in the chlorosome, together with their means and standard deviations; the middle column shows $A_{\parallel}(E)$ and $A_{\perp}(E)$ (characterizing SOLP spectroscopy) and also gives the single-chlorosome LD spectrum, while the right column presents the SOCD spectra for the four individual chlorosomes for three different values of the angle of incidence: $\xi = 0^{\circ}$, 45° , and 90° . From this, we see that the spectra for linear polarization have a very weak dependence on the average length of the aggregates inside the chlorosome, even for the smallest lengths. This is also true for CD spectroscopy with $\xi = 0^{\circ}$ and $\xi = 90^{\circ}$. By contrast, CD spectroscopy with $\xi = 45^{\circ}$ gives a clear variation of the spectra with the average aggregate length, despite the considerable variations in this length. This confirms the above conclusion that SOCD spectroscopy on individual chlorosomes may indeed probe differences in average aggregate length between chlorosomes if the angle of incidence is chosen close to $\xi = 45^{\circ}$.

B. Model with varying tubular radii

Thus far, we have presented results using one fixed value for the radius of the tubular BChl aggregates inside the chlorosomes. This simplifying assumption was made because it enabled us to isolate the effects of the aggregate length on the spectra, in particular, on the SOCD spectra. Moreover, it is known that the spectra of tubular aggregates obtained using linearly polarized light (such as SOLP spectra) are quite sensitive to the radius^{32,38} and less so to the length,³⁹ suggesting that in an experimental approach, radius information can first be obtained by SOLP spectroscopy, after which SOCD can be used to get information on the length of the aggregates. Indeed, this is exactly how the value for R used above was obtained:

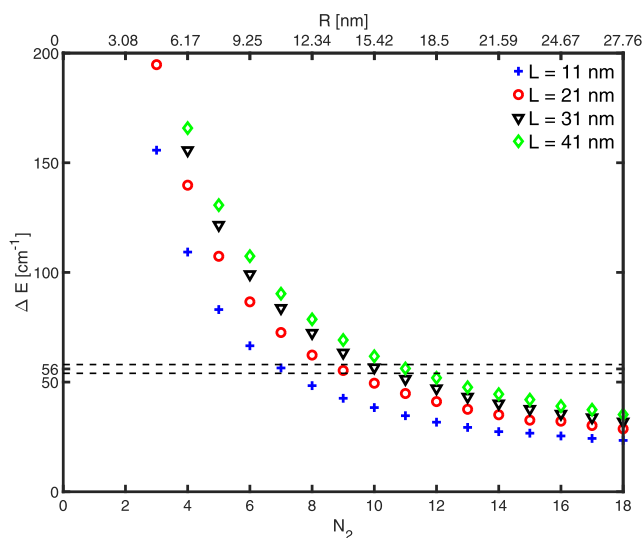


FIG. 6. Energy difference ΔE between parallel and perpendicular polarized energy bands as a function of radius (characterized by N_2 on the lower horizontal axis) for tubular aggregates of the structure applicable to chlorosomes, with different length, as indicated in the legend. The two dashed lines enclose four data points characterizing different (L, R) combinations with the same ΔE .

by averaging the radii obtained by analyzing SOLP spectra.⁴⁹ The method used to get information about the radius from experiments with linearly polarized light uses the notion that for long tubular aggregates, the energy separation ΔE between the main spectral bands polarized parallel and perpendicular to the tube's axis monotonically decreases with growing radius R .³² However, for tubular aggregates with finite length of up to about 50 or 100 nm, it has to be established to what extent the length affects ΔE . To this end, we simulated $A_{\parallel}(E)$ and $A_{\perp}(E)$ for tubular aggregates with the lattice structure fixed to the one used throughout this paper (Sec. II A) and varying length L and radius R (characterized by N_2) and obtained ΔE from them. Since some of the spectra, especially for small L and R (N_2), have satellite peaks [see Fig. S5 in the [supplementary material](#) (Note 4)], we calculated the average energy (weighted by the spectral intensity over the whole band) for both polarizations and took their difference as ΔE . The resulting data are presented in Fig. 6.

Figure 6 clearly shows that for all lengths considered, ΔE indeed monotonically decreases with the radius but that this relation itself depends on L as well. This implies that ΔE alone does not allow

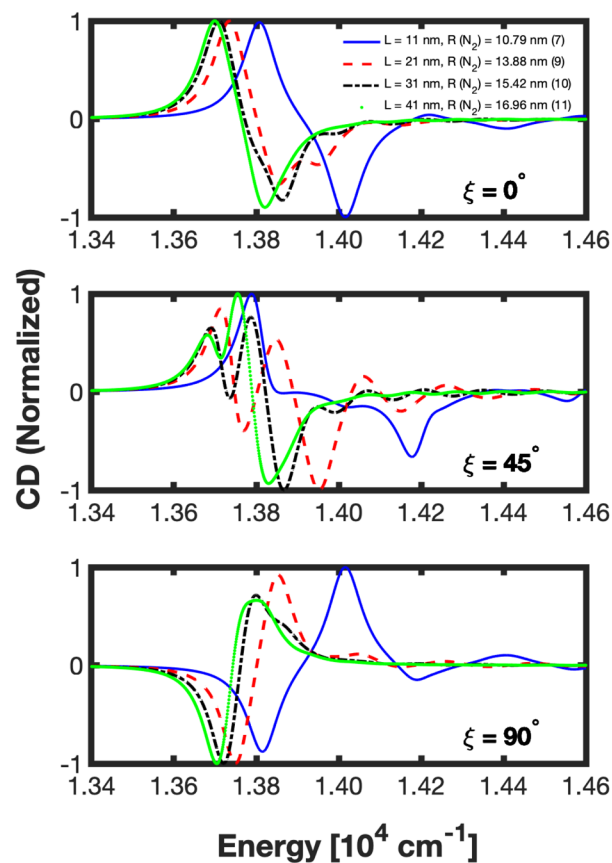


FIG. 7. SOCD spectra of tubular aggregates of the structure applicable to chlorosomes, calculated for the four combinations of length and radius, (L, R) , which give $\Delta E \approx 56 \text{ cm}^{-1}$ in Fig. 6. From top to bottom, the spectra correspond to the wave vector of the incident light making an angle with the tubular axis of $\xi = 0^{\circ}$, 45° , and 90° . Each SOCD spectra is normalized to its maximum absolute intensity.

a unique determination of the radius if the length is not known. Rather, measuring ΔE allows for a range of combinations of lengths and radii that might apply. As an illustration, consider the four data points in Fig. 6 lying between the dashed black lines, which represent tubular aggregates with (L, R) combinations (11, 10.79), (21, 13.88), (31, 15.42), and (41, 16.96) (all numbers in nm) that all have $\Delta E \approx 56 \text{ cm}^{-1}$. Importantly, however, the R dependencies for different lengths in Fig. 6 are seen not to cross each other, which keeps the possibility open that the combination of SOLP (ΔE) measurements and SOCD measurements may still allow one to get information on both the typical length and typical radius of the tubular aggregates in a particular chlorosome. This is confirmed by Fig. 7, in which we show the SOCD spectra for the four above (L, R) combinations for $\xi = 0^\circ$, $\xi = 45^\circ$, and $\xi = 90^\circ$. This figure shows that indeed the different (L, R) combinations with the same ΔE can be distinguished using SOCD spectroscopy and that, as before, this is best done using $\xi = 45^\circ$.

Similar to what we did in Sec. III A, we checked whether the above conclusion still holds if we allow for variation of L and R within an individual chlorosome or whether such variation washes out the spectral differences. Again, we assume that each chlorosome consists of 50 tubular aggregates and that now not only their lengths but also their radii are taken randomly from Poisson distributions with averages \bar{L} and \bar{R} , respectively. We used four sets of (\bar{L}, \bar{R}) combinations that equal the above four sets, which gave $\Delta E \approx 56 \text{ cm}^{-1}$ in case all aggregates inside an individual chlorosome are identical. The spectra for four chlorosomes randomly generated using these distributions were obtained by adding the spectra of the tubular aggregates within each chlorosome. The results are shown in Fig. 8. The left column presents the histograms for the aggregate lengths and radii found in each chlorosome, together with their means and standard deviations; the middle column shows the corresponding $A_{\parallel}(E)$ and $A_{\perp}(E)$ (characterizing SOLP spectroscopy) and also gives the single-chlorosome LD spectrum, while the right

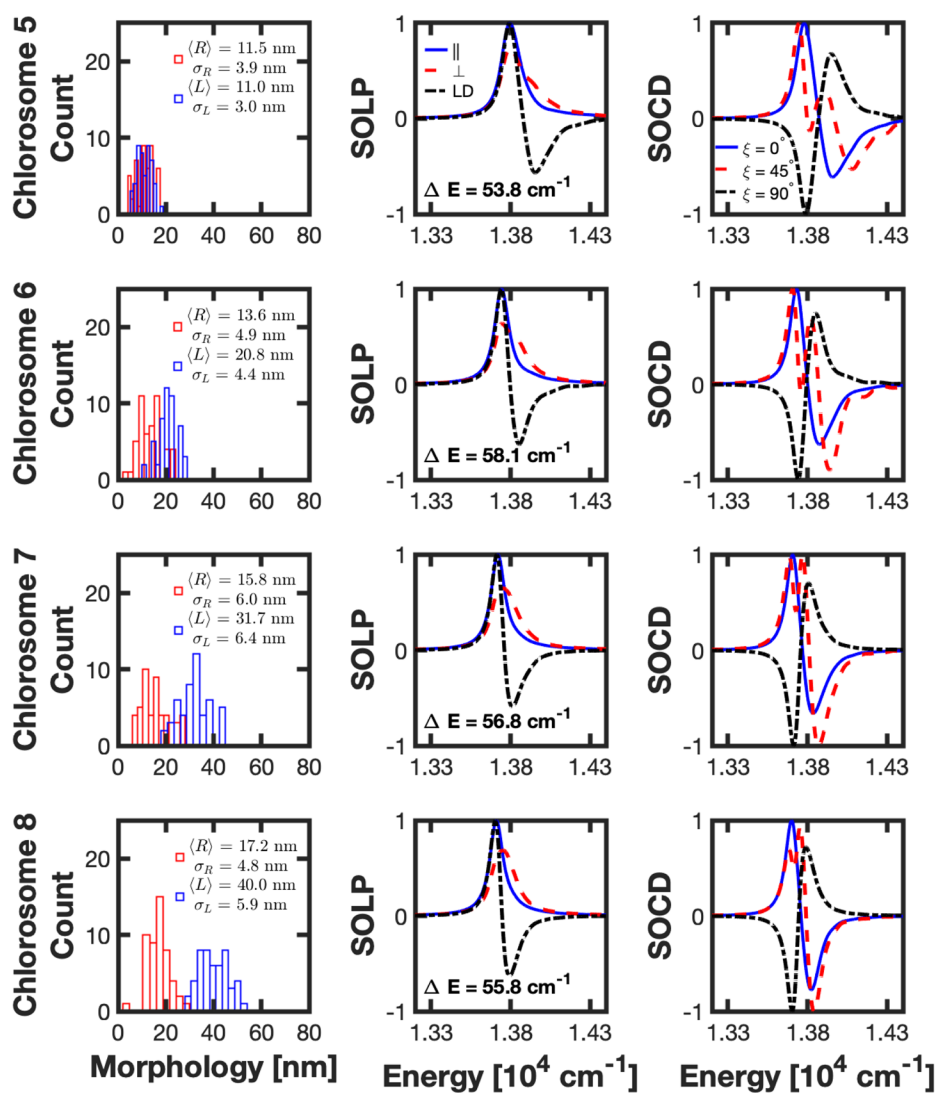


FIG. 8. Left column: histograms for the occurrences of the length (blue) and the radius (red) of the 50 tubular aggregates in four randomly generated chlorosomes using the Poisson distributions for L and R described in the text, with mean and standard deviation of each histogram as indicated. Middle column: SOLP spectra calculated for these individual chlorosomes, with light polarized parallel to the tubular axis [$A_{\parallel}(E)$, blue solid line] and perpendicular [$A_{\perp}(E)$, red dashed line]; the black dashed-dotted line shows the single-chlorosome LD spectrum. $A_{\parallel}(E)$ and $A_{\perp}(E)$ are normalized to the largest one of the two; each LD spectrum is normalized to its maximum absolute intensity. Right column: SOCD spectra $CD_{\xi}(E)$ calculated for these individual chlorosomes for three angles between the direction of incidence of the light and the chlorosome's tubular axis: $\xi = 0^\circ$ (solid blue line), 45° (red dashed line), and 90° (black dashed-dotted line). Each CD spectrum is normalized to its maximum absolute intensity.

column presents the SOCD spectra for the four individual chlorosomes for three different values of the angle of incidence: $\xi = 0^\circ$, 45° , and 90° .

The results in Fig. 8 show that the SOLP and LD spectra hardly differ for these four chlorosomes; specifically, analysis shows that they all indeed have a ΔE value close to 56 cm^{-1} . By contrast, the SOCD spectra are more sensitive to the ($\langle L \rangle$, $\langle R \rangle$) combination that applies if we use the setup with $\xi = 45^\circ$, even if the differences for the longer lengths are not as big as in Fig. 7. We note that the ability to distinguish different sets of lengths and radii generally increases with smaller dephasing rate and hence with lowering the temperature. The above results show that, in principle, the combination of SOLP and SOCD spectroscopy allows one to obtain estimates of the average length and average radius of the tubular aggregates within individual chlorosomes, even if these quantities vary for the aggregates inside each chlorosome according to Poisson distributions. We stress that our conclusions are not unique for the case presented here and can also be found for sets of chlorosomes with other pre-selected values of ΔE . To illustrate this, we present the results for four chlorosomes with $\Delta E \approx 40 \text{ cm}^{-1}$ in the [supplementary material](#) (Note 6).

IV. CONCLUSION

In this paper, we investigated theoretically how polarization dependent fluorescence excitation spectroscopy on single chlorosomes can provide information on the average (typical) size of the tubular aggregates that form the secondary structural elements inside these highly efficient light-harvesting organelles. We have found that a combination of single-chlorosome spectroscopies with linearly and circularly polarized light can be used to probe both the typical radius and the typical length of these aggregates. The ideal protocol scans the fluorescence excitation spectrum as a function of the polarization angle ϕ for linearly polarized light (SOLP spectroscopy), in combination with a scan of the single-chlorosome circular dichroism spectrum as a function of the angle ξ between the wave vector of the exciting light and the long axis of the chlorosome (SOCD spectroscopy). SOLP spectroscopy experiments have been used before to contribute to characterizing the structure of the aggregates, and these experiments were also used to estimate typical radii of the tubular aggregates in different chlorosomes.^{30,49} The SOLP spectra, however, show little dependence on the aggregate length, making this quantity inaccessible with linearly polarized light. We have shown in this paper that, by contrast, CD spectroscopy on individual chlorosomes is expected to be much more sensitive to the length. Moreover, we found that SOLP spectroscopy alone does not allow to uniquely determine the radius; it is the combination of both spectroscopies that allows probing both the typical radius and the typical length.

Single-object CD spectroscopy has only very rarely been applied, and as far as we know, no SOCD spectra have been taken of chlorosomes. It is to be expected that experimental constraints may make it hard to perform a full scan of the dependence of the spectrum on the angle ξ . Our calculations demonstrate that, in principle, making the measurement at two different angles provide all information and if also that turns out complicated, using $\xi = 45^\circ$ would be the best option. We have explained how the sensitivity of CD spectroscopy to the tubular length results from the interference

between so-called ring contributions and helical contributions to the spectrum, both of which yield dispersive (S-type) lineshapes with opposite overall sign, which partially overlap. The relative weight of both depends on the aggregate length, making the lineshape of the sum of these overlapping dispersive contributions highly sensitive to the length. Moreover, at $\xi = 0^\circ$ ($\xi = 90^\circ$), only helical (ring) contributions occur, while at intermediate angles, their linear combination determines the spectrum. This explains why using $\xi = 45^\circ$ by itself already provides much information.

The ability to resolve length and radius is limited by the width of the spectral contributions. If the width gets too large, it washes out the spectral structure that reflects the radius and especially the length. For aggregates with a short length and (or) a small radius, various spectral peaks are well resolved, leading to specific spectral structures that reflect the size, but for larger sizes, this becomes more challenging. For the homogeneous linewidth we used, this limits the lengths that can be resolved to about 50 nm. Using low-temperature conditions may help to reduce this linewidth and boost the resolution also for larger sizes. At the same time, having minimal inhomogeneous width also enhances the size sensitivity. This implies that for chlorosomes of mutants, which are known to have smaller inhomogeneity, the chances to resolve larger sizes are higher than for the wild-type chlorosomes.^{30,49}

In our model calculations, we adopted the picture that the dominant secondary structural elements inside the chlorosomes are tubular aggregates, all with the same molecular packing. We did this in order to isolate the effects of variations in length and radius of the tubular aggregates between different chlorosomes and hope that our observations and predictions will inspire new experiments on single chlorosomes. Of course, in reality the situation is more complicated: the packing may reveal disorder as well, leading to disorder in the molecular transition energies and the excitation transfer interactions, which, in turn, will affect the spectra. In addition, not all aggregates need to be tubular; other secondary structural elements may occur, such as lamellar and multi-walled tubular structures.⁶ Extending the current study to include such effects and investigate how robust the predicted sensitivity to average length and radius is for various additional sources of heterogeneity is an interesting and important topic for future research. Such extensions, however, are outside the scope of this work.

Finally, we note that the idea of combining ϕ dependent SOLP spectroscopy and ξ dependent SOCD spectroscopy also may be fruitful for other supramolecular structures where information on the variation of their internal structure is hard to obtain through other sources.

SUPPLEMENTARY MATERIAL

See the [supplementary material](#) for supporting information that provides further details or substantiates statements presented in the main text.

ACKNOWLEDGMENTS

The authors would like to thank Professor Dr. Thomas Renger and Dr. Dominik Lindorfer for helpful discussions. L.M.G. and J. Kö. acknowledge financial support from the State of Bavaria in

the framework of the Collaborative Research Network “Solar Technologies go Hybrid” and the Elite Network of Bavaria program “Macromolecular Science.”

The authors have no conflicts of interest to disclose.

DATA AVAILABILITY

The data that support the findings of this study are available from the corresponding author upon reasonable request.

REFERENCES

- H. van Amerongen, L. Valkunas, and R. van Grondelle, *Photosynthetic Excitons* (World Scientific, 2000).
- R. E. Blankenship, *Molecular Mechanisms of Photosynthesis* (Blackwell Science, 2002).
- A. F. Collings and C. Critchley, *Artificial Photosynthesis: From Basic Biology to Industrial Application* (Wiley-VCH, 2005).
- T. S. Balaban, H. Tamiaki, and A. R. Holzwarth, “Chlorins programmed for self-assembly,” in *Supermolecular Dye Chemistry* (Springer Berlin Heidelberg, Berlin, Heidelberg, 2005), pp. 1–38.
- P. Fromme, *Photosynthetic Protein Complexes: A Structural Approach* (Wiley-Blackwell, 2008).
- G. T. Oostergetel, H. van Amerongen, and E. J. Boekema, *Photosynth. Res.* **104**, 245 (2010).
- G. R. A. Kumara, S. Kaneko, M. Okuya, B. Onwona-Agyeman, A. Konno, and K. Tennakone, *Sol. Energy Mater. Sol. Cells* **90**, 1220 (2006).
- L. Hammarström and S. Hammes-Schiffer, *Acc. Chem. Res.* **42**(12), 1859 (2009), part of the Special Issue: Artificial Photosynthesis and Solar Fuels.
- P. I. Gordiichuk, G.-J. A. H. Wetzelaer, D. Rimmerman, A. Gruszka, J. W. de Vries, M. Saller, D. A. Gautier, S. Catarci, D. Pesce, S. Richter, P. W. M. Blom, and A. Herrmann, *Adv. Mater.* **26**, 4863 (2014).
- D. A. Bryant and D. P. Canniffe, *J. Phys. B: At., Mol. Opt. Phys.* **51**, 033001 (2018).
- R. R. Choubey, R. B. M. Koehorst, D. Bina, P. C. Struik, J. Pšenčík, and H. van Amerongen, *Biochim. Biophys. Acta, Bioenerg.* **1860**, 147 (2019).
- R. G. Saer and R. E. Blankenship, *Biochem. J.* **474**, 2107 (2017).
- A. R. Holzwarth, K. Griebenow, and K. Schaffner, *J. Photochem. Photobiol., A* **65**, 61 (1992).
- S. Sengupta, D. Ebeling, S. Patwardhan, X. Zhang, H. von Berlepsch, C. Böttcher, V. Stepanenko, S. Uemura, C. Hentschel, H. Fuchs, F. C. Grozema, L. D. A. Siebbles, A. R. Holzwarth, L. Chi, and F. Würthner, *Angew. Chem., Int. Ed.* **51**, 6378 (2012).
- D. M. Eisele, C. W. Cone, E. A. Bloemsmas, S. M. Vlaming, C. G. F. van der Kwaak, R. J. Silbey, M. G. Bawendi, J. Knoester, J. P. Rabe, and D. A. Vanden Bout, *Nat. Chem.* **4**, 655 (2012).
- L. A. Staehelin, J. R. Golecki, R. C. Fuller, and G. Drews, *Arch. Microbiol.* **119**, 269 (1978).
- L. A. Staehelin, J. R. Golecki, and G. Drews, *Biochim. Biophys. Acta, Bioenerg.* **589**, 30 (1980).
- J. M. Olson, *Biochim. Biophys. Acta, Rev. Bioenerg.* **594**, 33 (1980).
- R. E. Blankenship, J. M. Olson, and M. Miller, “Antenna complexes from green photosynthetic bacteria,” in *Anoxygenic Photosynthetic Bacteria* (Kluwer Academic Publishers: Springer, Dordrecht, The Netherlands, 1995), pp. 399–435.
- J. M. Olson, *Photochem. Photobiol.* **67**, 61 (1998).
- N.-U. Frigaard and D. A. Bryant, “Chlorosomes: Antenna organelles in photosynthetic green bacteria,” in *Complex Intracellular Structures in Prokaryotes* (Springer Berlin Heidelberg, Berlin, Heidelberg, 2006), pp. 79–114.
- J. M. Linnanto and J. E. I. Korppi-Tommola, *J. Phys. Chem. B* **117**, 11144 (2013).
- J. Pšenčík, T. P. Ikonen, P. Laurinmäki, M. C. Merckel, S. J. Butcher, R. E. Serimaa, and R. Tuma, *Biophys. J.* **87**, 1165 (2004).
- G. T. Oostergetel, M. Reus, A. Gomez Maqueo Chew, D. A. Bryant, E. J. Boekema, and A. R. Holzwarth, *FEBS Lett.* **581**, 5435 (2007).
- J. M. Linnanto and J. E. I. Korppi-Tommola, *Photosynth. Res.* **96**, 227 (2008).
- S. Ganapathy, G. T. Oostergetel, P. K. Wawrzyniak, M. Reus, A. Gomez Maqueo Chew, F. Buda, E. J. Boekema, D. A. Bryant, A. R. Holzwarth, and H. J. M. de Groot, *Proc. Natl. Acad. Sci. U. S. A.* **106**, 8525 (2009).
- S. Ganapathy, G. T. Oostergetel, M. Reus, Y. Tsukatani, A. Gomez Maqueo Chew, F. Buda, D. A. Bryant, A. R. Holzwarth, and H. J. M. de Groot, *Biochemistry* **51**, 4488 (2012).
- J. Alster, M. Kabeláč, R. Tuma, J. Pšenčík, and J. V. Burda, *Comput. Theor. Chem.* **998**, 87 (2012).
- J. Pšenčík, S. J. Butcher, and R. Tuma, “Chlorosome: Structure, function and assembly,” in *The Structural Basis of Biological Energy Generation* (Springer Netherlands, Dordrecht, 2014), pp. 77–109.
- L. M. Günther, M. Jendry, E. A. Bloemsmas, M. Tank, G. T. Oostergetel, D. A. Bryant, J. Knoester, and J. Köhler, *J. Phys. Chem. B* **120**, 5367 (2016).
- X. Li, F. Buda, H. J. M. de Groot, and G. J. A. Sevink, *J. Phys. Chem. C* **123**, 16462 (2019).
- C. Didraga, A. Pugžlys, P. R. Hania, H. von Berlepsch, K. Duppen, and J. Knoester, *J. Phys. Chem. B* **108**, 14976 (2004).
- N. J. Hestand, R. Tempelaar, J. Knoester, T. L. C. Jansen, and F. C. Spano, *Phys. Rev. B* **91**, 195315 (2015).
- N. J. Hestand and F. C. Spano, *Acc. Chem. Res.* **50**, 341 (2017).
- A. Löhner, T. Kunsel, M. I. S. Röhr, T. L. C. Jansen, S. Sengupta, F. Würthner, J. Knoester, and J. Köhler, *J. Phys. Chem. Lett.* **10**, 2715 (2019).
- A. S. Bondarenko, I. Patmanidis, R. Alessandri, P. C. T. Souza, T. L. C. Jansen, A. H. de Vries, S. J. Marrink, and J. Knoester, *Chem. Sci.* **11**, 11514 (2020).
- C. Spitz, J. Knoester, A. Ouart, and S. Daehne, *Chem. Phys.* **275**, 271 (2002).
- B. Kriete, A. S. Bondarenko, V. R. Jumde, L. E. Franken, A. J. Minnaard, T. L. C. Jansen, J. Knoester, and M. S. Pshenichnikov, *J. Phys. Chem. Lett.* **8**, 2895 (2017).
- C. Didraga, J. A. Klugkist, and J. Knoester, *J. Phys. Chem. B* **106**, 11474 (2002).
- V. I. Prokhorenko, D. B. Steensgaard, and A. R. Holzwarth, *Biophys. J.* **85**, 3173 (2003).
- C. Didraga and J. Knoester, *J. Chem. Phys.* **121**, 946 (2004).
- C. Chuang, C. K. Lee, J. M. Moix, J. Knoester, and J. Cao, *Phys. Rev. Lett.* **116**, 196803 (2016).
- A. S. Bondarenko, T. L. C. Jansen, and J. Knoester, *J. Chem. Phys.* **152**, 194302 (2020).
- F. Vacha, L. Bumba, D. Kaftan, and M. Vacha, *Micron* **36**, 483 (2005).
- S. Furumaki, F. Vacha, S. Habuchi, Y. Tsukatani, D. A. Bryant, and M. Vacha, *J. Am. Chem. Soc.* **133**, 6703 (2011).
- M. Jendry, T. J. Aartsma, and J. Köhler, *J. Phys. Chem. Lett.* **3**, 3745 (2012).
- R. Camacho, D. Täuber, and I. G. Scheblykin, *Adv. Mater.* **31**, 1805671 (2019).
- L. M. Günther, J. Knoester, and J. Köhler, *Molecules* **26**, 899 (2021).
- L. M. Günther, A. Löhner, C. Reiher, T. Kunsel, T. L. C. Jansen, M. Tank, D. A. Bryant, J. Knoester, and J. Köhler, *J. Phys. Chem. B* **122**, 6712 (2018).
- J. A. Betti, R. E. Blankenship, L. V. Natarajan, L. C. Dickinson, and R. C. Fuller, *Biochim. Biophys. Acta, Bioenerg.* **680**, 194 (1982).
- R. J. van Dorssen, H. Vasmel, and J. Amesz, *Photosynth. Res.* **9**, 33 (1986).
- K. Griebenow, A. R. Holzwarth, F. van Mourik, and R. van Grondelle, *Biochim. Biophys. Acta, Bioenerg.* **1058**, 194 (1991).
- K. Matsuura, M. Hirota, K. Shimada, and M. Mimuro, *Photochem. Photobiol.* **57**, 92 (1993).
- J. Martiskainen, J. Linnanto, R. Kananavičius, V. Lehtovuori, and J. Korppi-Tommola, *Chem. Phys. Lett.* **477**, 216 (2009).
- J. Martiskainen, J. Linnanto, V. Aumanen, P. Myllyperkiö, and J. Korppi-Tommola, *Photochem. Photobiol.* **88**, 675 (2012).
- S. Furumaki, Y. Yabiku, S. Habuchi, Y. Tsukatani, D. A. Bryant, and M. Vacha, *J. Phys. Chem. Lett.* **3**, 3545 (2012).
- R. Hassey, E. J. Swain, N. I. Hammer, D. Venkataraman, and M. D. Barnes, *Science* **314**, 1437 (2006).

- ⁵⁸R. Hassey, K. D. McCarthy, E. Swain, D. Basak, D. Venkataraman, and M. D. Barnes, *Chirality* **20**, 1039 (2008).
- ⁵⁹Y. Tang, T. A. Cook, and A. E. Cohen, *J. Phys. Chem. A* **113**, 6213 (2009).
- ⁶⁰M. D. Barnes, R. H. Paradise, E. Swain, and D. Venkataraman, *J. Phys. Chem. A* **113**, 9757 (2009).
- ⁶¹K. Katayama, S. Hirata, and M. Vacha, *Phys. Chem. Chem. Phys.* **16**, 17983 (2014).
- ⁶²E. Vinegrad, D. Vestler, A. Ben-Moshe, A. R. Barnea, G. Markovich, and O. Cheshnovsky, *ACS Photonics* **5**, 2151 (2018).
- ⁶³P. Spaeth, S. Adhikari, L. Le, T. Jollans, S. Pud, W. Albrecht, T. Bauer, M. Caldarola, L. Kuipers, and M. Orrit, *Nano Lett.* **19**, 8934 (2019).
- ⁶⁴E. A. Bloemsmas, S. M. Vlaming, V. A. Malyshev, and J. Knoester, *Phys. Rev. Lett.* **114**, 156804 (2015).
- ⁶⁵It should be pointed out that the precise value of E_{mol} does not influence our conclusions, as it mostly sets a reference value for the energy (frequency) axes in the spectra; it has no influence on the absorption lineshapes for linearly polarized light and a very small influence on the CD lineshapes (as those depend on the absolute wavelength).
- ⁶⁶Y. Tian, R. Camacho, D. Thomsson, M. Reus, A. R. Holzwarth, and I. G. Scheblykin, *J. Am. Chem. Soc.* **133**, 17192 (2011).
- ⁶⁷H. van Amerongen, H. Vasmel, and R. van Grondelle, *Biophys. J.* **54**, 65 (1988).
- ⁶⁸G. Garab and H. van Amerongen, *Photosynth. Res.* **101**, 135 (2009).
- ⁶⁹D. Lindorfer and T. Renger, *J. Phys. Chem. B* **122**, 2747 (2018).
- ⁷⁰P. Akhtar, D. Lindorfer, M. Lingvay, K. Pawlak, O. Zsiros, G. Siligardi, T. Jávorfí, M. Dorogi, B. Ughy, G. Garab, T. Renger, and P. H. Lambrev, *J. Phys. Chem. B* **123**, 1090 (2019).
- ⁷¹O. J. G. Somsen, R. van Grondelle, and H. van Amerongen, *Biophys. J.* **71**, 1934 (1996).
- ⁷²J. Dostál, T. Maňal, R. Augulis, F. Vácha, J. Pšenčík, and D. Zigmantas, *J. Am. Chem. Soc.* **134**, 11611 (2012).
- ⁷³MATLAB R2015b, Random numbers for the length are obtained by using the `poissrnd` command, The MathWorks Inc., Natick, Massachusetts, 2015.